Progress In Electromagnetics Research, Vol. 171, 171–184, 2021

Mechanisms and Modeling of 2D-Materials-Based Resistive Random Access Memory Devices

Hao Xie[1, 2], Zhili Wang[3], Yanbin Yang[4], Xiaohui Hu[1], Hong Liu[1], and Wei Qi[1, *]

(*Invited Review*)

Abstract—Resistive random access memory (RRAM) devices are promising candidates for next generation high capacity data storage due to their superior properties such as cost-effective fabrication, high operating speed, low power consumption, and long data retention. Particularly, the two dimensional (2D)-materials-based RRAM has attracted researchers' attention because of its unique physical and chemical properties without the constraint of lattice matching. In this review, the switching mechanisms and modeling of RRAM devices based on the 2D materials such as hexagonal-boron nitride (h-BN) and graphene are discussed. Firstly, the monolayer and multilayer h-BN RRAMs are introduced, and their mechanisms and compact model are further described. Then, the mechanisms of graphene electrode-based RRAM (GE-RRAM) for different applications are also introduced and compared. Furthermore, the electrical conductivity, multi-physic and compact models of GE-RRAM are introduced. This review paper provides the guidance for the design and optimization of the 2D-materials-based RRAM in the next generation memories.

1. INTRODUCTION

The mechanism of resistive random access memory (RRAM) is resistance switching through the conductive filament growth and rupture which is controlled by applied voltage [1–5]. The most common resistance switching materials are transition metal oxides, such as HfO_x, TiO_x, ZnO_x, WO_x, TaO_x, NiO_x, and AlO_x [6–14]. However, RRAM with traditional resistance switching materials has some problems such as large reading current, low integration density, and big power consumption. Recently, 2D-materials-based RRAMs using h-BN resistance switching layer and graphene electrode become a research hotspot due to their large on-off current ratio, low power consumption, stable high resistive state (HRS) and low resistive state (LRS) resistances, and good mechanical properties [15–20].

Various novel RRAM structures using h-BN resistance switching material have been proposed for solving the problems in traditional RRAM. In 2018, Wang et al. reported that multiple weak-filaments in h-BN RRAM are formed by defective paths in the crystalline structure [18]. In 2018, Ranjan et al. proposed a simple model based on drift-diffusion principle to explain resistance switching mechanisms of multilayer h-BN RRAM [21]. Besides, there are also many h-BN RRAMs with good performance [18, 21, 24–27]. In 2019, Wu et al. observed characteristics of free formation and large on-off current ratio in monolayer h-BN RRAM [22]. In 2019, Zhu et al. reported the first 2D-materials-based memristors with switchingstably between two or three resistive states for multiple

Received 8 October 2021, Accepted 7 December 2021, Scheduled 13 December 2021

* Corresponding author: Wei Qi (qiw@zucc.edu.cn).

[1] School of Information and Electrical Engineering, Zhejiang University City College, Hangzhou 310015, China. [2] Innovative Institute of Electromagnetic Information and Electronic Integration (EIEI), College of Information Science and Electronic Engineering, Zhejiang University, Hangzhou 310027, China. [3] Science and Technology on Electromagnetic Compatibility Laboratory, China Ship Development and Design Centre, Wuhan 430064, China. [4] Zhijiang Intelligence Institute in Chengdu Tianfu District, Chengdu 610213, China.

storage applications [23]. In 2021, Zhuang et al. reported that the rupture of conductive filaments one by one is probably governed by Joule heating effect rather than electrical field [24].

Moreover, many RRAM problems such as scalability and power consumption can be solved by using graphene electrodes. In 2013, Tian et al. proposed a low power consumption RRAM with single-layer graphene inserted between TiN/Ti electrode and oxide [28]. In 2015, Lee et al. inserted a defective graphene layer between oxide film and metal electrode to control the formation and rupture of conductive filament [29]. In 2015, Lee et al. proposed a GE-RRAM to improve the performance [30]. In 2016, Lee et al. demonstrated that the movement of oxygen ions can be controlled by modulating the opening of graphene nanopores [31]. In 2020, our research group developed the electrical conductivity model of graphene electrode and further built multi-physical model by solving current transport equation, oxygen vacancy migration equation, and heat conduction equation [32]. In 2020, Alimkhanuly et al. built a compact model of GE-RRAM to fit experimental I-V characteristics and study electric potential distribution [33].

In this review paper, we introduce and discuss the mechanisms of several different 2D-materials-based RRAM devices, in which the corresponding merits are also discussed. Besides, multi-physic and compact models of both *h*-BN and graphene-based RRAM devices are presented and discussed, which are consistent with the experimental results. Finally, a conclusion is given.

2. *h*-BN RRAM

In this section, different *h*-BN-based RRAM devices are introduced, and their mechanisms and compact models are further described.

2.1. *h*-BN Resistance Switching Material

h-BN is regarded as an ideal 2D insulator material owing to its excellent properties such as large band gap and outstanding thermal characteristics [19, 34–38]. Recently, the resistance switching phenomenon was reported in both monolayer and multilayer *h*-BN RRAM devices [18, 19, 22, 39–43].

2.1.1. Monolayer h-BN

Due to the excessive leakage current, there is no nonvolatile resistance switching phenomenon in the vertical metal-insulator-metalstructure [22, 40, 44]. Wu et al. observed nonvolatile resistance switching effect in monolayer *h*-BN RRAM with vertical metal electrodes as shown in Fig. 1(a) [22]. Monolayer *h*-BN atomic transistors show the characteristic of free formation, and its on-off current ratio is up to 10^7 [22].

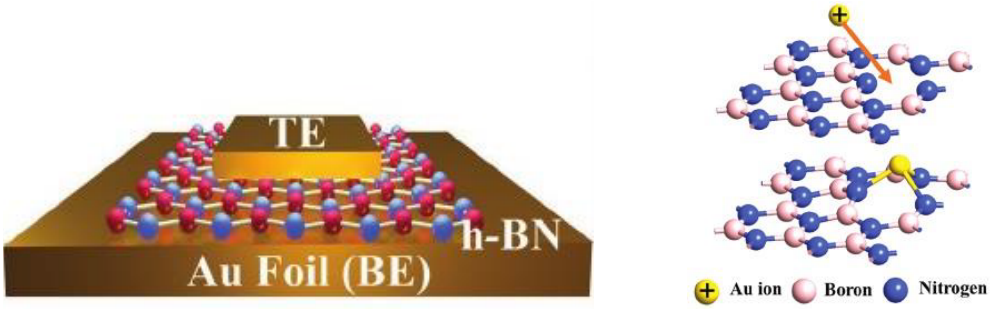

Figure 1. (a) Schematic of monolayer *h*-BN MIM sandwich structure. (b) Top: the initial states of simulation. Bottom: the final state of gold ion and boron vacancies in monolayer *h*-BN [22].

Boron and nitrogen vacancies generally exist in *h*-BN sheets, which have great impact on electronic conduction. The mechanisms of resistance switching are explained by ab-initio simulation results [22].

The simulated initial structure is a single-layer h-BN sheet with boron vacancies and a positive gold ion as shown in Fig. 1(b).

During the set process, the gold atoms migrate under the applied voltage, meanwhile, losing the electrons and becoming gold ions with positive charge. Interaction in the h-BN can be represented as,

$$\mathrm{Au} \rightarrow \mathrm{Au}^{+} + e^{-} \tag{1}$$

Moreover, the ions are attracted by boron vacancies and then reduced by the process as in Eq. (2). As a result, the conductive paths in the vertical direction are formed, and the low resistive state (LRS) can be established.

$$\mathrm{Au}^{+} + e^{-} \rightarrow \mathrm{Au} \tag{2}$$

Multilevel switching can be implemented at different compliant currents, thus realizing multiple storage applications.

2.1.2. Multilayer h-BN

Zhu et al. reported the first 2D material-based memristors for multiple storage applications, which can switch between each two or three stable resistive states by using the current limitation (CL) and reset voltage [23, 45]. The multilayer h-BN stack sandwich RRAM device consists of Au/Ti/Graphene/h-BN/Graphene/Au/Ti/SiO_2/Si, as shown in Fig. 2.

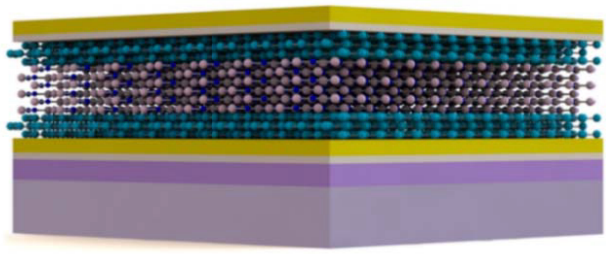

Figure 2. Schematic of multilayer h-BN sandwich RRAM [23].

Three stable resistive states can be realized due to the formation of a narrower conductive filament across the multilayer h-BN, as shown in Fig. 3(d). An intermediate state named soft-low resistive state (S-LRS) is generated between the HRS and LRS. Thus, the device can switch among three resistive states of HRS, S-LRS, and LRS, while CL is 1 mA, and its I-V curves are given in Fig. 3(b).

2.2. Model

Although 2-D materials like h-BN have aroused great interest, RRAM based on 2-D materials is very scarce in the market [46]. In addition, analytical tools that can describe and predict RRAM performance are also deficient, which are necessary for the design and measurement of 2D-materials-based RRAM [47].

2.2.1. Multiple Conductive Filaments in h-BN RRAM

Wang et al. reported that multiple weak-filaments in h-BN RRAM are formed by defective paths in the crystalline structure [18]. Zhuang et al. reported that the rupture of conductive filaments is probably governed by Joule heating effect rather than electrical field [24], and the possible schematic diagram is shown in Fig. 4.

Ranjan et al. proposed a simple model based on drift-diffusion principle as shown in Fig. 5 to explain resistance switching mechanisms of multilayer h-BN RRAM [21]. During the set process, the boron ions move towards the Pt electrode on which a high voltage is applied as shown in Fig. 5(a), thus leaving boron vacancies inside h-BN to form conduction filaments. During the reset process, a low voltage is applied on the Pt electrode, and boron ions are pushed back from the Pt electrode to h-BN to annihilate the boron vacancies, resulting in the rupture of conduction filament as shown in Fig. 5(b). The directional movement of boron ions is controlled by the interaction between diffusion and drift.

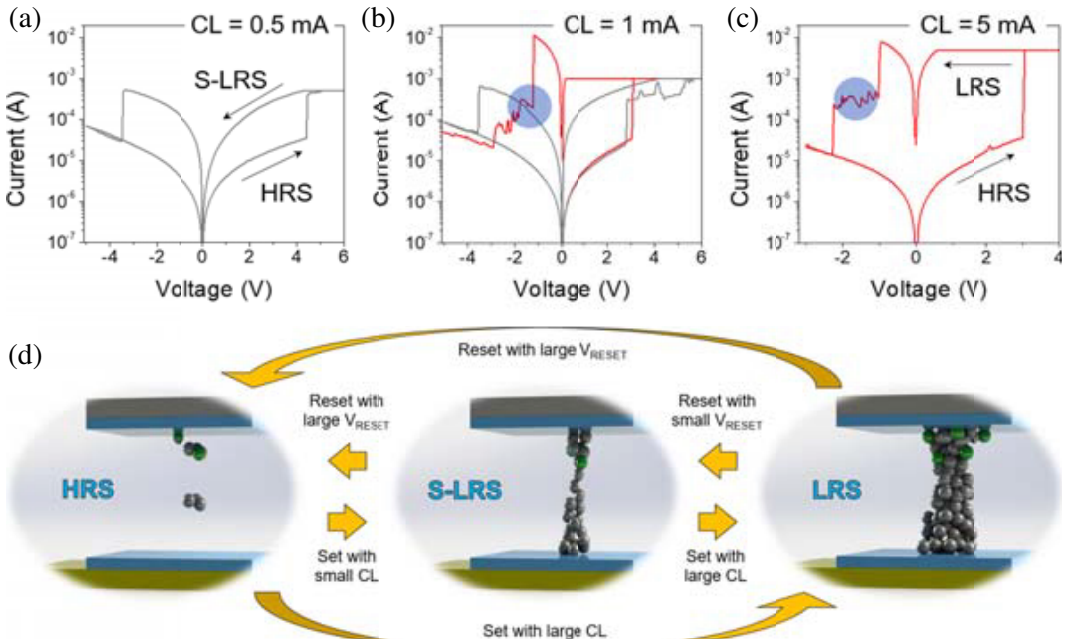

Figure 3. I-V curve of the *h*-BN sandwich RRAM [23] (a) in HRS and S-LRSas CL is 0.5 mA, (b) in three resistance switching states (HRS, S-LRS and LRS) as CL is 1 mA and (c) in LRS and HRS as CL is 5 mA. (d) Schematic of different resistance switching states (HRS, S-LRS and LRS).

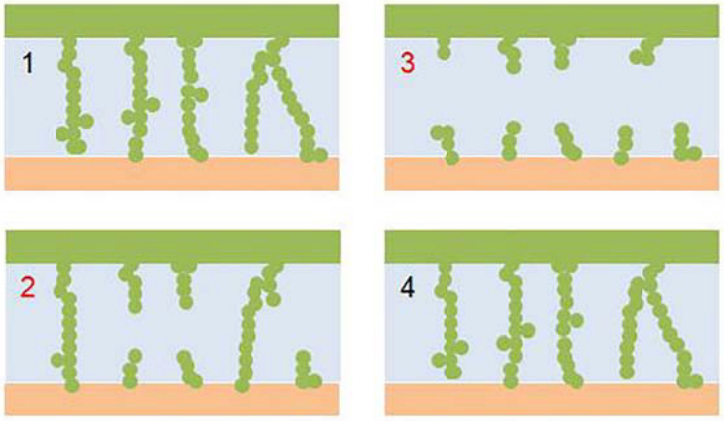

Figure 4. The possible evolution of conductive filament [24].

2.2.2. Compact Model

Pan et al. built a compact model based on the nonlinear Landauer approach which accurately describes the functions of *h*-BN stack sandwich RRAM device as show in Fig. 2. The corresponding I-V characteristics of forming, set and reset processes got by the proposed compact model are shown in Fig. 6, and they are consistent with the experimental results [47].

The current through N independent conductive filaments of multilayer *h*-BN can be described as Eq. (3) [47].

$$I = I^+ - I^- \tag{3}$$

$$I^+ = \frac{2e}{h}\sum_{i=1}^{N}\int_{-\infty}^{+\infty} T_i(E,V)f[E-\beta_i eV]dE \tag{4}$$

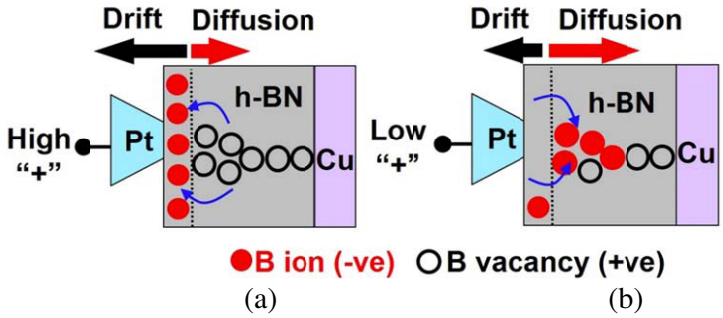

Figure 5. (a) The set process. (b) Reset process of the resistance switching mechanisms based on drift-diffusion principle, where black and red balls are boron vacancies and ions, respectively [21].

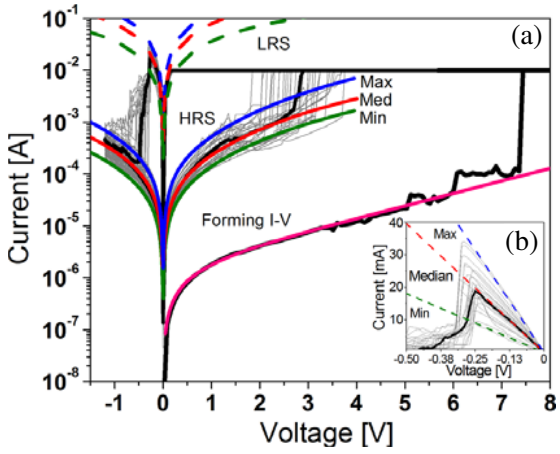

Figure 6. The I-V characteristics between experiment and model [47]. (a) IV curves of forming process using Eq. (1). (b) IV curves of HRS and LRS using Eq. (2).

$$I^{-} = \frac{2e}{h}\sum_{i=1}^{N}\int_{-\infty}^{+\infty} T_i(E,V) f[E-(1-\beta_i)eV]dE \tag{5}$$

where I^{+} and I^{-} are the right- and left-going current components, respectively. T_i is the transmission probability for CF_i, and f is the Fermi-Dirac distribution function. V is the applied voltage, and E is the energy measured from the equilibrium fermi level.

During the forming progress, the tunneling barrier in the h-BN is large, the transmission probability can be approximated as [47],

$$T(E,V) \approx \exp[\alpha(E-\varphi)] \tag{6}$$

where ϕ and α are the height and width of the confinement potential barrier, respectively.

There are series of resistance effects in the h-BN RRAM devices with multiple conductive filaments. The current during the forming progress can be described as [47],

$$I = \frac{1}{\alpha e R_s}\left\{\frac{1}{\beta}W\left\{\frac{N\beta R_s}{R_0}\exp[\alpha(\beta eV-\varphi)]\right\}\right\} + \frac{1}{1-\beta}W\left\{-\frac{N(1-\beta)R_s}{R_0}\exp[-\alpha((1-\beta)eV+\varphi)]\right\} \tag{7}$$

where W is the Lambert function, and R_s is the series resistance.

During the set and reset progresses, the current can be solved by using the circuit model and Thévenin transformation [47], which is given by,

$$I = \frac{VG_p - I_0}{1+R_sG_p} + \frac{1}{\alpha eR_s}W\left\{\frac{\alpha eI_0R_s}{1+R_sG_p}\exp\left[\frac{\alpha e(V+R_sI_0)}{1+R_sG_p}\right]\right\} \tag{8}$$

$$G_p = G_0 n \tag{9}$$

$$I_0 = \frac{2e(N-n)}{\alpha h} \exp(-\alpha\varphi) \tag{10}$$

3. GRAPHENE RRAM

In this section, the RRAM mechanisms of different GE-RRAMs are firstly introduced. Then, multi-physic and compact models of GE-RRAM are further described [32, 33, 48, 49].

3.1. Graphene Electrode

The most common electrode materials in RRAM are conventional metals such as Al, Cu, Au, Pt, and active metals such as Ti and Ni [50–56]. Oxygen atoms accumulate near the conventional metal electrode, resulting in a large current, which will then generate Joule heat and make the conductive filament reputed [57]. On the contrary, oxygen atoms can migrate into active metal electrode under bias voltage, and as a result, the conductive filament will be formed near the active metal electrode [55]. However, large leakage current will occur in the initial state, which will affect the service life of RRAM devices. To solve the above problems, researchers have proposed many GE-RRAMs to optimize the performance of RRAM [23, 28–31, 46, 58–64].

3.1.1. Blocking Graphene Layer

Tian et al. proposed an RRAM structure with single-layer graphene inserted between TiN/Ti electrode and oxide by using the impermeability of graphene, as shown in Fig. 7(a) [28]. Fig. 7(c) shows the schematic diagram of oxygen ions movement mechanisms during set and reset processes. During the set process, the oxygen ions move towards the interface between TiN/Ti electrode and oxide under the action of electric field as shown in Fig. 7(c) [28]. Due to the impermeability of single-layer graphene, oxygen ions

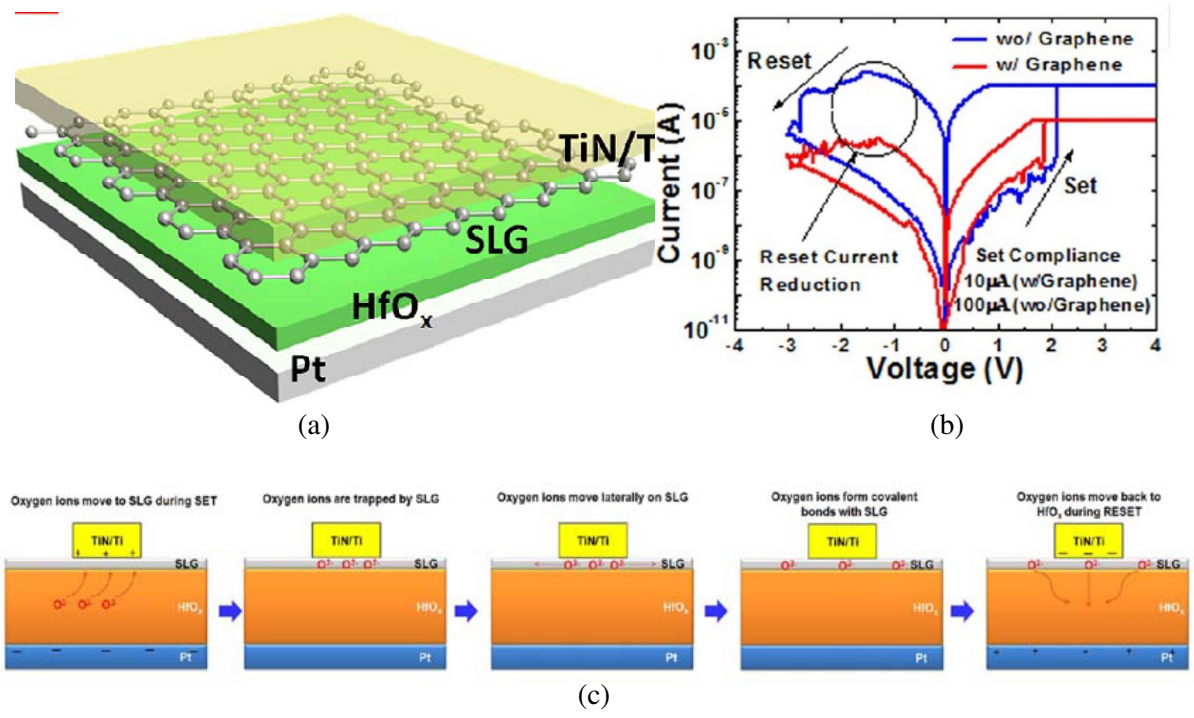

Figure 7. (a) Structure of RRAM. (b) Resistance switching behavior of RRAMs. (c) Schematic diagrams of oxygen ions movement mechanisms [28].

cannot migrate into Ti electrode, but enter the single-layer graphene. Oxygen ions form covalent bonds with graphene defects, and this process is reversible during the reset process [57]. Fig. 7(b) shows the resistive switching behavior of RRAMs with and without single-layer graphene. The significant current reduction of graphene RRAM is obtained during the reset process, due to the large low resistance state resistance caused by the single-layer graphene.

3.1.2. Defective Graphene Layer

The randomness growing and rupture processes of conductive filament lead to the instability switching parameters during different cycles [57, 58]. In order to solve this problem, Lee et al. inserted a defective graphene layer between oxide film and metal electrode to control the formation and rupture of conductive filament as shown in Fig. 8 [29]. The specific defects in the graphene monolayer are generated by Ar^+ ion assisted reaction system, inducing broken C-C bonds [29]. The growing region of conductive filament can be controlled by inducing confirmed current path distribution in the oxide. The switching voltages range of metal-graphene-insulator-metal (MGIM) in both reset and set processes is small, and its HRS and LRS resistances are more stable as shown in Fig. 9. Therefore, defective graphene electrode can reduce fluctuations in switching parameters, and further improve the service life of RRAM [30, 59].

Lee et al. further demonstrated that the movement of oxygen ions can be controlled by modulating the opening of graphene nanopores on Pd/Ta/Graphene/Ta_2O_5/Pd RRAM as shown in Fig. 10 [31]. Only oxygen ions near the opening of nanopores can migrate through, leaving oxygen vacancies to form the conductive filament, as shown in Fig. 10(c). Therefore, the position and diameter of conductive filament can be perfectly controlled relying on the location and size of the engineered nanopores on graphene. Furthermore, the operation current is significantly decreased during the set and reset processes as shown in Fig. 10(c). The smaller the size of the engineered nanopores is, the larger its resistance is, resulting in a smaller current in the RRAM [57].

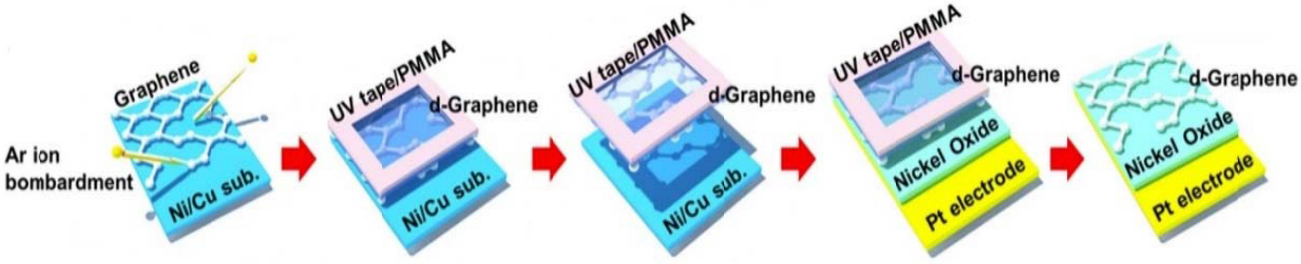

Figure 8. Illustration of fabrication process for MGIM structure [29].

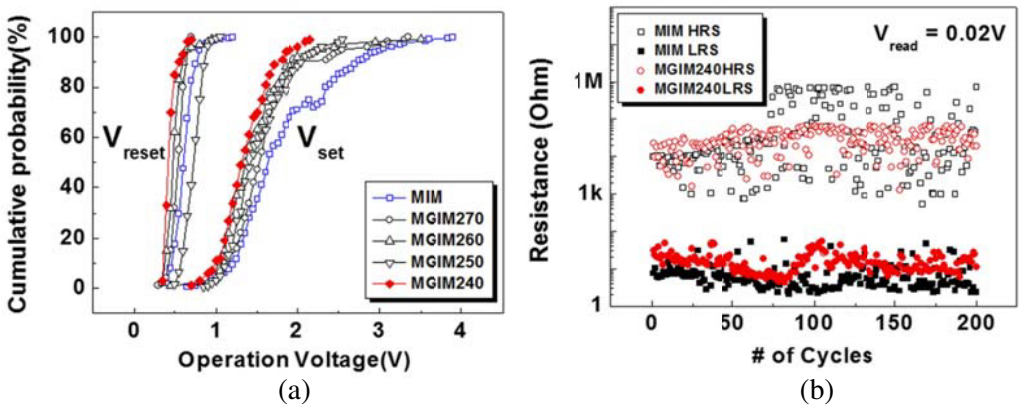

Figure 9. Experimental measurements between MGIM and normal RRAM [29]. (a) Cumulative probability of switching voltages. (b) Resistances at HRS and LRS.

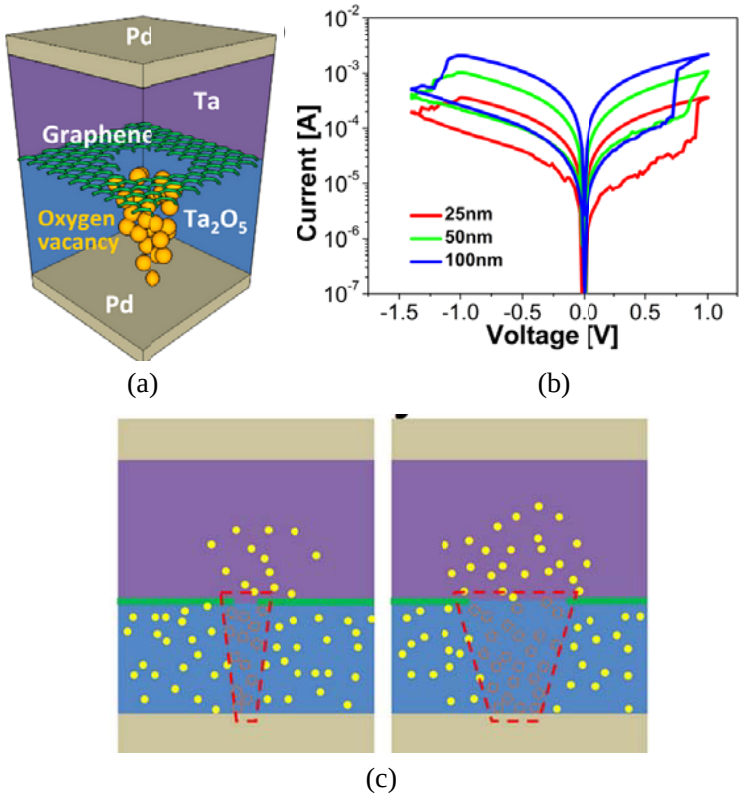

Figure 10. (a) Structure of Pd/Ta/graphene/Ta_2O_5/Pd RRAM. (b) I-V characteristic with different sizes of the engineered nanopores. (c) Schematic of the formation of conductive filament with different nanopores sizes [31].

3.1.3. Graphene Edge Electrode

Many novel vertical RRAMs such as plane electrode (Pt)/HfO_x/pillar electrode (TiN) (Pt-RRAM) structure have been developed to increase their integration density [65]. However, the thickness of each insulating material cannot be less than a safe value to avoid cross-talk from adjacent cell [66].

Lee et al. proposed a graphene edge electrode RRAM to improve the performance as shown in Fig. 11(a) [30]. The contact mode between graphene and oxide is edge contact, and the edge contact resistance is much smaller than that of conventional Pt-RRAM. Besides, its power consumption is 300

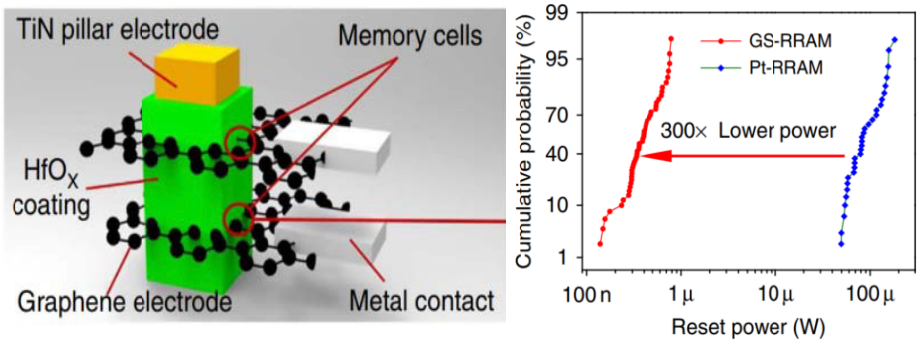

Figure 11. (a) Schematic structure of GE-RRAM. (b) Reset power distribution of GE-RRAM and Pt-RRAM [30].

times lower than that of Pt-RRAM as shown in Fig. 11(b) [30]. Besides, the integration of RRAM is highly increased because the thickness of monolayer graphene is only 0.3 nm.

Our research group studied the mechanism of GE-RRAM and established its multi-physical simulation model [32]. Different from conventional Pt-RRAM, the oxygen ions can migrate horizontally into graphene electrode rather than accumulating near the electrode during the set process. Part of the oxygen ions react with carbon atoms and form graphene oxide with different oxidation degrees. As a result, the leaving oxygen vacancies in the resistive switching material HfO_x form conductive filament [30]. The sp^3 structure is introduced into the graphene due to the covalent cross linking during the formation of graphene oxide, which leads to the decrease of its electrical conductivity [67]. During the reset process, oxygen ions return from the graphene electrode to metal oxide, causing the rupture of conductive filament.

3.2. Model

Researches on the GE-RRAM are mostly based on experiments. However, modeling and simulation of GE-RRAM to provide physical insight and guide for its optimization design are also very meaningful.

3.2.1. Multi-Physic Model

Our research group developed the electrical conductivity model of graphene electrode with different degrees of oxidation [32]. Further, the in-house developed finite difference algorithm is used to solve the current transport, oxygen vacancy migration, and heat conduction equations to simulate the GE-RRAM cell.

From the particle conservation law, the number of oxygen atoms in the graphene electrode is equal to that of the oxygen vacancies in HfO_x, which is given by

$$V \cdot n(\vec{r}, t) = S \cdot o(\vec{r}, t) \tag{11}$$

where V is the volume of conductive filament, S the area of graphene oxide, $n(\vec{r}, t)$ the oxygen vacancy density of HfO_x, and $o(\vec{r}, t)$ the oxygen atoms density of graphene oxide.

The electrical conductivity of graphene oxide is highly dependent on its degree of oxidation [32]. An electrical conductivity model of graphene oxide, in which the conductivity is exponentially dependent on the density of oxygen atoms in the partially oxidized graphene oxide, is proposed as follows,

$$\sigma_{ox}(\vec{r}, t) = \sigma_o e^{(-r \times o(\vec{r}, t))} \tag{12}$$

where σ_o is the electrical conductivity of pure graphene, r a constant, and $o(\vec{r}, t)$ the oxygen atoms density of graphene oxide.

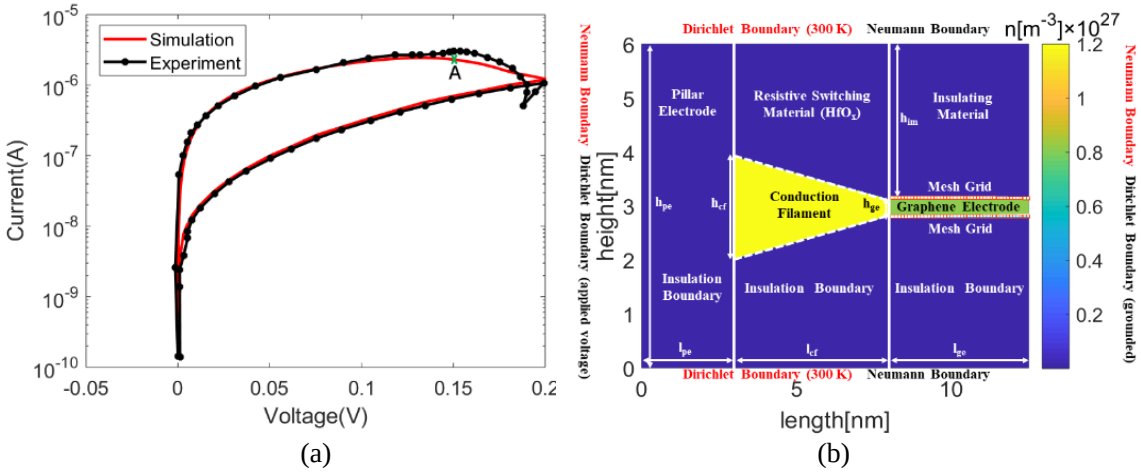

Figure 12. (a) The reset I-V characteristics of the GE-RRAM in simulation and experiment. (b) Oxygen vacancy density distributions and boundary conditions [32].

The I-V curves and oxygen vacancy distribution are investigated numerically by building a multi-physic model as shown in Fig. 12 [32].

3.2.2. Compact Model

Alimkhanuly et al. built a compact model of GE-RRAM to simulate the I-V characteristics and further study electric potential distributions [33]. The development of the conductive filament can be described by vertical and horizontal growths.

Firstly, the horizontal evolution of the conduction path can be described as the grow or rupture of the conductive filament. The tunneling gap distance variation can be used to accurately demonstrate the RRAM resistance switching process of the GE-RRAM model as shown in Fig. 11 [33].

$$I = I_0 \times \exp\left(\frac{-d_{gap}}{d_0}\right) \times \sinh\left(\frac{V}{V_0}\right) \tag{13}$$

where V is the applied voltage, and d_{gap} is the tunneling gap distance.

Secondly, the vertical evolution of the conduction path can be modeled as an increase or decrease in the width of conductive filament. The geometrical shape of conductive filament in the GE-RRAM model can be modeled as a cylinder or truncated cone. The current density is linearly related to the diameter of conductive filament because of the dominant Ohmic nature of the conduction path [33].

$$I = \pi d_{CF}^2 \cdot V/(4\rho \cdot t_{ox}) \tag{14}$$

where t_{ox} is the thickness of oxide, and ρ and d_{CF} are the resistivity and diameter of the conductive filament, respectively.

The I-V characteristics of GE-RRAM obtained by compact model and experiment are shown in Fig. 13(a), which are in good agreement.

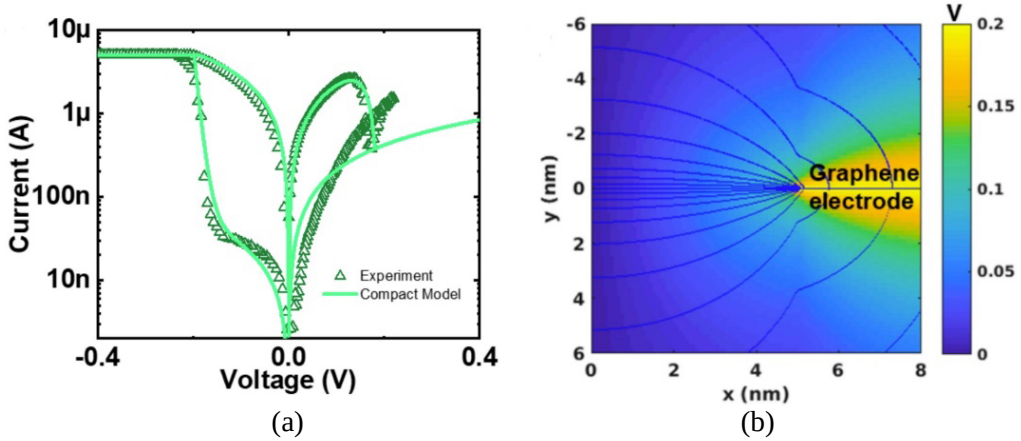

Figure 13. (a) The I-V characteristics of GE-RRAM got by compact model and experiment. (b) The electric potential of GE-RRAM [33].

4. CONCLUSION

In summary, many promising 2D-materials-based RRAM devices have been recently uncovered that deserve further exploration. In particular, we have highlighted novel *h*-BN and graphene-based RRAM devices in this review paper. Compared to ordinary RRAM, the free formation, large on-off current ratio, three stable resistive states, etc. properties of *h*-BN-based RRAM and low power consumption, stable HRS and LRS resistance, etc. properties of graphene-based RRAM make them have strong competitive power in the memory fields. Multi-physic and compact models of both *h*-BN and graphene-based RRAM devices are consistent with the experimental results, which provide physical insight and guide for their optimization design. The mechanisms and modeling of 2D-materials-based RRAM devices discussed above represent a crucial step toward the realization for future high density RRAM applications.

ACKNOWLEDGMENT

The work is supported by the Zhejiang Provincial Natural Science Foundation of China under Grant No. LQ22F010002, the National Natural Science Foundation of China under Grants No. 92066105, and by the Sichuan Science and Technology Program No. 2021YJ0087.

REFERENCES

1. Yang, J. J., D. B. Strukov, and D. R. Stewart, "Memristive devices for computing," *Nature Nanotech.*, Vol. 8, No. 1, 13–24, 2013.
2. Wong, H.-S. P. and S. Salahuddin, "Memory leads the way to better computing," *Nature Nanotech.*, Vol. 10, No. 3, 191–195, 2015.
3. Fong, S. W., C. M. Neumann, and H.-S. P. Wong, "Phase-change memory towards a storage-class memory," *IEEE Trans. Electron Devices*, Vol. 64, No. 11, 4374–4385, 2017.
4. Yu, S. M., X. M. Guan, and H. S. P. Wong, "On the stochastic nature of resistive switching in metal oxide RRAM: Physical modeling, monte carlo simulation, and experimental characterization," *2011 IEEE International Electron Devices Meeting (IEDM)*, 2011.
5. Wang, X. F., H. M. Zhao, Y. Yang, and T. L. Ren, "Graphene resistive random memory — The promising memory device in next generation," *Chinese Physics B*, Vol. 26, No. 3, 038501, 2017.
6. Paolo, L., R. Rosario, and I. Fernanda, "Forming kinetics in HfO_2-based RRAM cells," *IEEE Trans. Electron Devices*, Vol. 60, No. 1, 438–443, 2013.
7. Kim, S. and Y. K. Choi, "A comprehensive study of the resistive switching mechanism in Al/TiOx/TiO_2/Al-structured RRAM," *IEEE Trans. Electron Devices*, Vol. 56, No. 12, 3049–3054, 2009.
8. Kumar, D., U. Chand, L. W. Siang, and T. Y. Tseng, "High-performance TiN/Al_2O_3/ZnO/Al_2O_3/TiN flexible RRAM device with high bending condition," *IEEE Trans. Electron Devices*, Vol. 67, No. 2, 493–498, 2020.
9. Chien, W. C., Y. C. Chen, E. K. Lai, Y. D. Yao, P. Lin, S. F. Horng, J. Gong, T. H. Chou, H. M. Lin, M. N. Chang, Y. H. Shih, K. Y. Hsieh, R. Liu, and C.-Y. Lu, "Unipolar switching behaviors of RTO WOX RRAM," *IEEE Electron Devices Letters*, Vol. 31, No. 2, 126–128, 2010.
10. Sung, C., et al., "Investigation of I-V linearity in TaOx-based RRAM devices for neuromorphic applications," *IEEE Journal of The Electron Devices Society*, Vol. 7, No. 1, 404–408, 2019.
11. Xie, H. W., Y. T. Liu, and Z. X. Huang, "A NiOx, based threshold switching selector for RRAM crossbar array application," *2019 IEEE International Conference on Electron Devices and Solid-State Circuits (EDSSC)*, 2019.
12. Woo, J., et al., "Improved synaptic behavior under identical pulses using AlOx/HfO_2 bilayer RRAM array for neuromorphic systems," *IEEE Electron Devices Letters*, Vol. 37, No. 8, 994–997, 2016.
13. Wedig, A., M. Luebben, D.-Y. Cho, M. Moors, K. Skaja, V. Rana, T. Hasegawa, K. K. Adepalli, B. Yildiz, R. Waser, and I. Valov, "Nanoscale cation motion in TaOx, HfOx and TiOx," *Nature Nanotech.*, Vol. 11, No. 1, 67–75, 2016.
14. Lu, N. D., P. X. Sun, L. Li, Q. Liu, S. B. Long, H. B. Lv, and M. Liu, "Thermal effect on endurance performance of 3-dimensional RRAM crossbar array," *Chinese Physics B*, Vol. 25, No. 5, 1–5, 2016.
15. Sohn, J., S. Lee, Z. Jiang, H. Y. Chen, and H. S. P. Wong, "Atomically thin graphene plane electrode for 3D RRAM," *2014 IEEE International Electron Devices Meeting (IEDM)*, 2014.
16. Yu, S., H. Y. Chen, B. Gao, J. Kang, and H. S. P. Wong, "HfOx-based vertical resistive switching random access memory suitable for bit-cost-effective three-dimensional cross-point architecture," *ACS Nano*, Vol. 7, No. 3, 2320–2325, 2013.
17. Ji, Y., S. Lee, B. Cho, S. Song, and T. Lee, "Flexible organic memory devices with multilayer graphene electrodes," *ACS Nano*, Vol. 5, No. 7, 5995–6000, 2011.
18. Wang, C. H., et al., "3D monolithic stacked 1T1R cells using monolayer MoS_2 FET and hBN RRAM fabricated at low (150 degrees C) temperature," *2018 IEEE International Electron Devices Meeting (IEDM)*, 2018.

19. Pan, C. B., et al., "Coexistence of grain-boundaries-assisted bipolar and threshold resistive switching in multilayer hexagonal boron nitride," *Adv. Funct. Mater.*, Vol. 27, No. 10, 1604811, 2017.
20. Zhuang, P. P., et al., "Nonpolar resistive switching of multilayer-hBN-based memories," *Adv. Electron. Mater.*, Vol. 6, No. 1, 1900979, 2020.
21. Ranjan, A., N. Raghavan, S. J. O'Shea, S. Mei, M. Bosman, K. Shubhakar, and K. L. Pey, "Conductive atomic force microscope study of bipolar and threshold resistive switching in 2D hexagonal boron nitride films," *Scientific Reports*, Vol. 8, 2854, 2018.
22. Wu, X. H., et al., "Thinnest nonvolatile memory based on monolayer h-BN," *Adv. Mater.*, Vol. 31, No. 15, 1806790, 2019.
23. Zhu, K. C., et al., "Graphene-boron nitride-graphene cross-point memristors with three stable resistive states," *ACS Applied Materials & Interfaces*, Vol. 11, No. 41, 37999–38005, 2019.
24. Zhuang, P. P., W. Z. Ma, J. Liu, W. W. Cai, and W. Y. Lin, "Progressive RESET induced by Joule heating in hBN RRAMs," *Appl. Phys. Lett.*, Vol. 118, No. 14, 143101, 2021.
25. Lin, W. Y., P. P. Zhuang, D. Akinwande, X. A. Zhang, and W. W. Cai, "Oxygen-assisted synthesis of hBN films for resistive random access memories," *Applied Phys. Letters*, Vol. 115, No. 7, 073101, 2019.
26. Palumbo, F., et al., "Bimodal dielectric breakdown in electronic devices using chemical vapor deposited hexagonal boron nitride as dielectric," *Advanced Electronic Materials*, Vol. 4, No. 3, 1700506, 2018.
27. Jiang, J. K., K. Parto, W. Cao, and K. Banerjee, "Ultimate monolithic-3D integration with 2D materials: Rationale, prospects, and challenges," *IEEE Journal of The Electron Devices Society*, Vol. 7, No. 1, 878–887, 2019.
28. Tian, H., H. Y. Chen, B. Gao, S. Yu, J. Liang, Y. Yang, D. Xie, J. Kang, T. L. Ren, Y. Zhang, and W. H. S. Philip, "Monitoring oxygen movement by raman spectroscopy of resistive random access memory with a graphene-inserted electrode," *NANO Letters*, Vol. 13, 651–657, 2013.
29. Lee, K., et al., "Enhancement of resistive switching under confined current path distribution enabled by insertion of atomically thin defective monolayer graphene," *Sci. Rep.*, Vol. 5, 11279, 2015.
30. Lee, S., J. Sohn, Z. Z. Jiang, H. Y. Chen, and H. -S. P. Wong, "Metal oxide-resistive memory using graphene-edge electrodes," *Nature Commu.*, Vol. 6, 8407, 2015.
31. Lee, J., C. Du, K. Sun, E. Kioupakis, and W. D. Lu, "Tuning ionic transport in memristive devices by graphene with engineered nanopores," *ACS Nano*, Vol. 10, No. 3, 3571–3579, 2016.
32. Xie, H., W. C. Chen, S. Zhang, G. D. Zhu, A. Khaliq, J. Hu, and W. Y. Yin, "Modeling and simulation of resistive random access memory with graphene electrode," *IEEE Trans. Electron Devices*, Vol. 67, No. 3, 915–921, 2020.
33. Alimkhanuly, B., S. Kim, L. W. Kin, and S. Lee, "Electromagnetic analysis of vertical resistive memory with a sub-nm thick electrode," *Nanomaterials*, Vol. 10, No. 9, 1634, 2020.
34. Dean, C. R., A. F. Young, I. Meric, C. Lee, L. Wang, S. Sorgenfrei, K. Watanabe, T. Taniguchi, P. Kim, K. L. Shepard, and J. Hone, "Boron nitride substrates for high-quality graphene electronics," *Nat. Nanotechnol.*, Vol. 5, No. 10, 722–726, 2010.
35. Giovannetti, G., P. A. Khomyakov, G. Brocks, P. J. Kelly, and J. van den Brink, "Substrate-induced band gap in graphene on hexagonal boron nitride:Ab initio density functional calculations," *Phys. Rev. B*, Vol. 76, No. 7, 073103, 2007.
36. Weng, Q. H., X. B. Wang, X. Wang, Y. Bando, and D. Golberg, "Functionalized hexagonal boron nitride nanomaterials: Emerging properties and applications," *Chem. Soc. Rev.*, Vol. 45, No. 12, 3989–4012, 2016.
37. Lee, J., T. J. Ha, K. N. Parrish, S. F. Chowdhury, L. Tao, A. Dodabalapur, and D. Akinwande, "High-performance current saturating graphene field-effect transistor with hexagonal boron nitride dielectric on flexible polymeric substrates," *IEEE Electron Device Lett.*, Vol. 34, No. 2, 172–174, 2013.

38. Jiang, Y., X. Lin, and H. Chen, "Directional polaritonic excitation of circular, huygens and Janus dipoles in graphene-hexagonal boron nitride heterostructures," *Progress In Electromagnetics Research*, Vol. 170, 169–176, 2021.
39. Shi, Y., C. Pan, V. Chen, N. Raghavan, K. L. Pey, F. M. Puglisi, E. Pop, H. S. P. Wong, and M. Lanza, "Coexistence of volatile and non-volatile resistive switching in 2D h-BN based electronic synapses," *2017 IEEE International Electron Devices Meeting (IEDM)*, 2017.
40. Tsai, T. M., et al., "Controlling the degree of forming soft-breakdown and producing superior endurance performance by inserting BN-based layers in resistive random access memory," *IEEE Electron Devices Letters*, Vol. 38, No. 4, 445–448, 2017.
41. Zhang, D. J., C. H. Yeh, W. Cao, and K. Banerjee, "0.5T0.5R — An ultracompact RRAM cell uniquely enabled by van der Waals heterostructures," *IEEE Trans. Electron Devices*, Vol. 68, No. 4, 2033–2040, 2021.
42. Jeong, H., et al., "Resistive switching in few-layer hexagonal boron nitride mediated by defects and interfacial charge transfer," *ACS Applied Materials & Interfaces*, Vol. 12, No. 41, 46288–46295, 2020.
43. Tan, C. L. and H. Zhang, "Two-dimensional transition metal dichalcogenide nanosheet-based composites," *Chem. Soc. Rev.*, Vol. 44, No. 9, 2713–2731, 2015.
44. Rehman, M. M., H. M. N. U. Rehman, J. Z. Gul, W. Y. Kim, K. S. Karimov, and N. Ahmed, "Decade of 2D-materials-based RRAM devices: A review," *Science and Technology of Advanced Materials*, Vol. 21, No. 1, 147–186, 2020.
45. Chiang, C. C., V. Ostwal, P. Wu, C. S. Pang, F. Zhang, Z. H. Chen, and J. Appenzeller, "Memory applications from 2D materials," *Applied Physics Reviews*, Vol. 8, No. 2, 021306, 2021.
46. Huang, Y. J. and S. C. Lee, "Graphene/h-BN heterostructures for vertical architecture of rram design," *Scientific Reports*, Vol. 7, 9679, 2017.
47. Pan, C. B., et al., "Model for multi-filamentary conduction in graphene/hexagonal-boron-nitride/graphene based resistive switching devices," *2D Materials*, Vol. 4, No. 2, 025099, 2017.
48. Zhang, H. H., P. P. Wang, S. Zhang, L. Li, P. Li, W. E. I. Sha, and L. J. Jiang, "Electromagnetic-circuital-thermal multiphysics simulation method: A review," *Progress In Electromagnetics Research*, Vol. 169, 87–101, 2020.
49. Duan, H., W. Fang, W.-Y. Yin, E. Li, and W. Chen, "Computational investigation of nanoscale semiconductor devices and optoelectronic devices from the electromagnetics and quantum perspectives by the finite difference time domain method," *Progress In Electromagnetics Research*, Vol. 170, 63–78, 2021.
50. Seo, S., J. Lim, S. Lee, B. Alimkhanuly, A. Kadyrov, D. Jeon, and S. Lee, "Graphene-edge electrode on a Cu-based chalcogenide selector for 3D vertical memristor cells," *ACS Appl. Mater. Interfaces*, Vol. 11, No. 46, 43466–43472, 2019.
51. Bai, Y., H. Wu, K. Wang, R. Wu, L. Song, T. Li, J. Wang, Z. Yu, and H. Qian "Stacked 3D RRAM array with graphene/CNT as edge electrodes," *Sci. Rep.*, Vol. 5, 13785, 2015.
52. Mannequi, C., A. Delamoreanu, L. Latu-Romain, V. Jousseaume, H. Grampeix, S. David, C. Rabot, A. Zenasni, C. Vallee, and P. Gonona, "Graphene-HfO_2-based resistive RAM memories," *Microelectronic Engineering*, Vol. 161, 82–86, 2016.
53. Zhao, H., H. Tu, F. Wei, and J. Du, "Highly transparent dysprosium oxide-based RRAM with multilayer graphene electrode for low-power nonvolatile memory application," *IEEE Trans. Electron Dev.*, Vol. 61, No. 5, 1388–1393, 2014.
54. Yao, J., J. Lin, Y. Dai, G. Ruan, Z. Yan, L. Li, L. Zhong, D. Natelson, and J. M. Tour, "Highly transparent nonvolatile resistive memory devices from silicon oxide and graphene," *Nature Commu.*, Vol. 3, 1101, 2012.
55. Yang, K., W. Y. Chang, P. Y. Teng, S. F. Jeng, S. J. Lin, P. W. Chiu, and J. H. He, "Fully transparent resistive memory employing graphene electrodes for eliminating undesired surface effects," *Proc. IEEE*, Vol. 101, No. 7, 1732–1739, 2013.

56. Hui, F., E. Grustan-Gutierrez, S. Long, Q. Liu, A. K. Ott, A. C. Ferrari, and M. Lanza "Graphene and related materials for resistive random access memories," *Adv. Electron. Mater.*, Vol. 3, No. 8, 600195, 2017.
57. Liu, Y., S. B. Long, Q. Liu, H. B. Lv, and M. Liu, "Resistive switching performance improvement via modulating nanoscale conductive filament, involving the application of two-dimensional layered materials," *Small*, Vol. 13, No. 35, 1604306, 2017.
58. Kim, J., D. Kim, Y. Jo, J. Han, H. Woo, H. Kim, K. K. Kim, J. P. Hong, and H. Im, "Impact of graphene and single-layer BN insertion on bipolar resistive switching characteristics in tungsten oxide resistive memory," *Thin Solid Films*, Vol. 589, 188–193, 2015.
59. Qian, M., Y. Pan, F. Liu, M. Wang, H. Shen, D. He, B. Wang, Y. Shi, F. Miao, and X. Wang, "Tunable, ultralow-power switching in memristive devices enabled by a heterogeneous graphene-oxide interface," *Adv. Mater*, Vol. 26, No. 20, 3275–3281, 2014.
60. Jung, I., D. A. Dikin, R. D. Piner, and R. S. Rouff, "Tunable electrical conductivity of individual graphene oxide sheets reduced at "low" temperatures," *Nano Letters*, Vol. 8, No. 12, 4283–4287, 2008.
61. Pan, F., S. Gao, C. Chen, C. Song, and F. Zeng, "Recent progress in resistive random access memories: Materials, switching mechanisms, and performance," *Materials Science & Engineering R-Reports*, Vol. 83, 1–59, 2014.
62. Chen, X., et al., "Controlled nonvolatile transition in polyoxometalates-graphene oxide hybrid memristive devices," *Adv. Mater. Technol.*, Vol. 4, No. 3, 1800551, 2019.
63. Chen, C., C. Song, J. Yang, F. Zeng, and F. Pan, "Oxygen migration induced resistive switching effect and its thermal stability in W/TaOx/Pt structure," *Appl. Phys. Lett.*, Vol. 100, No. 25, 253509, 2012.
64. Chen, H. Y., et al., "Experimental study of plane electrode thickness scaling for 3D vertical resistive random access memory," *Nanotechnology*, Vol. 24, No. 46, 465201, 2013.
65. Li, S., W. Chen, Y. Luo, J. Hu, P. Gao, J. Ye, K. Kang, H. Chen, E. Li, and W. Y. Yin, "Fully coupled multiphysics simulation of crosstalk effect in bipolar resistive random access memory," *IEEE Trans. Electron Devices*, Vol.9, No. 64, 3647–3653, 2017.
66. Wan, S. and Q. Cheng, "Role of interface interactions in the construction of GO-based artificial nacres," *Adv. Materials Interfaces*, Vol. 5, No. 12, 1800107, 2018.
67. Punckt, C., F. Muckel, S. Wolff, I. A. Aksay, C. A. Chavarin, G. Bacher, and W. Mertin, "The effect of degree of reduction on the electrical properties of functionalized graphene sheets," *Appl. Phys. Lett.*, Vol. 102, No. 2, 023114, 2013.